Proceedings of the 21st ICSMGE, Vienna, Austria, 14 – 19 June 2026. Pistrol, Adam & Schweiger (eds.)
Published by: ÖGG, Austrian Society for Geomechanics, Salzburg, Austria, ISBN 978-3-9503898-4-5
https://doi.org/10.53243/ICSMGE2026-143

Precise Liquefaction Assessment and Damage Mitigation of a Shopping Center by Accounting for Soil Fabric Effect

Nikolay Yordanov Milev
Department of Geotechnics, University of Architecture, Civil Engineering and Geodesy, Bulgaria, milev_fte@uacg.bg

Juan José Briones Contreras
Institute of Industrial Science, The University of Tokyo, Japan, briones@g.ecc.u-tokyo.ac.jp

Kwok-Kwan Lau
Institute of Technology, Shimizu Corporation, Japan, joannelau@shimz.co.jp

ABSTRACT: This study addresses the assessment and mitigation of liquefaction risk at a planned shopping center site in Septemvri, Bulgaria, where shallow foundations on spread footings will support a precast single-storey concrete superstructure. The site's geological profile includes a problematic clayey sand layer, approximately 2.0 meters thick, situated below groundwater at a depth of about 3.5 meters. Composition-based criteria confirmed the material's susceptibility to liquefaction. Detailed site-specific evaluation using Standard Penetration Tests (SPT) and shear wave velocity (V_s) measurements via the down-hole method indicated that this layer could liquefy under the Ultimate Limit State (ULS) earthquake scenario, according to Eurocode 8, but not under the Damage Limit State (DLS). To improve assessment accuracy, a new integrated approach was applied that combines density information from SPT with soil fabric effects from V_s. Using this method, no liquefaction was predicted even for ULS. However, given its novelty, a conservative design approach was adopted. The ground beneath all spread footings was improved using unreinforced Deep Soil Mixing (DSM) columns to provide vertical support and resist lateral loads from surrounding potentially liquefied soil. Outside the building footprint (such as for floor slabs and parking areas) no additional ground improvement was implemented, as DLS conditions showed no liquefaction risk. This targeted mitigation ensures structural safety and life protection during a large earthquake, while optimizing costs and construction scope.

KEYWORDS: soil liquefaction, liquefaction countermeasure, soil fabric, earthquake geotechnical engineering, deep soil mixing.

1 INTRODUCTION

This study addresses the seismic liquefaction risk for a planned shopping center in the town of Septemvri, Bulgaria. The site is located on the elevated southern terrace of the Maritsa River within a seismic zone, with a reference peak ground acceleration $a_g = 0.23g$, exceeding the Eurocode 8 (ECS, 2004) screening threshold of $0.15g$ for liquefaction assessment.

The objective was to evaluate liquefaction susceptibility and potential deformations for both Ultimate Limit State (ULS) and Damage Limit State (DLS) conditions, and to design appropriate mitigation measures. The assessment was carried out using procedures based on Standard Penetration Tests (SPT) data and shear wave velocity (V_s) measurements, providing complementary insights into soil density and fabric. Based on the results, targeted soil improvement only beneath the spread footings was implemented using the deep soil mixing (DSM) method, aiming to ensure structural safety under severe seismic loading while optimizing construction costs.

2 SITE CONDITIONS AND INVESTIGATION

The project site covers approximately 7,000 m^2 of flat terrain in the town of Septemvri, with ground elevations between 234 m and 235 m a.s.l. It is occupied by single-storey structures, concrete pavements, and grassed areas, some formerly used for agriculture. Surrounding development consists mainly of residential and commercial buildings, most over 50 years old. Existing structures and pavements will be demolished, and subsurface utilities of mixed condition were encountered during investigation. According to the GIS liquefaction hazard map of the Bulgarian Ministry of Regional Development and Public Works (Nakov & Dobrev, 2014), the site lies within a medium liquefaction hazard zone. The investigation included nine boreholes, in-situ SPTs, and down-hole seismic testing for shear wave velocity (V_s), with laboratory tests on selected disturbed and undisturbed samples, depending on their intended use.

Figure 1. Regional and site location: (top) liquefaction hazard zones in Bulgaria with project site – (Nakov & Dobrev, 2014); (middle) satellite view; (bottom) site plan with investigation points.

The subsurface profile consists of three main soil units of Neogene–Quaternary age, as follows:

- Layer 1: organic clay or artificial fill (0.7–1.6 m thick), composed of organics, gravel, crushed stone, and construction debris, unsuitable for foundation bearing.
- Layer 2: gravel and sand (locally silty or clayey), with relatively high stiffness and strength, forming the primary bearing stratum for the planned foundations.
- Layer 3: clayey sand / sandy clay, occurring as a 0.7–2.2 m thick interlayer within Layer 2, with low stiffness and strength, and water-saturated.

Groundwater was encountered at a depth of about 3.5 m, with potential seasonal rise up to 2.0 m. The presence of loose, saturated granular soils and low-plasticity sandy clays in the profile, combined with a design peak ground acceleration of 0.23*g*, indicates a code-relevant potential for liquefaction, particularly within the weaker interlayer (Layer 3).

Figure 1 presents the regional and site location, including liquefaction hazard mapping, satellite imagery, and the layout of investigation points (IP1, IP2, and IP3). These three locations, selected from the nine boreholes drilled on site, are the focus of this study as they provide both Standard Penetration Test (SPT) data and shear wave velocity (V_s) measurements for direct comparison.

Down-hole geophysical testing was conducted to obtain semi-direct measurements of shear wave velocity (V_s) in accordance with (ASTM, 2019). The method involves lowering a triaxial borehole geophone into a PVC-cased hole and generating polarized S-waves at the surface using a shear beam struck alternately from opposite sides. Polarity reversal allows reliable identification of S-wave first arrivals, which were picked from corrected seismograms at each depth.

The velocity calculation procedure is illustrated in Figure 2 (left). Corrected travel time is computed as:

$$t_c = D\frac{t}{R} \tag{1}$$

The velocity for each depth interval is determined as:

$$V_d = \frac{\Delta D}{\Delta t_c} \tag{2}$$

where D is depth, t the measured arrival time, R the source–receiver offset, ΔD the depth interval, and Δt_c the corresponding corrected time difference.

Two seismic units (SU1 and SU2) were identified based on trends. SU1, present to ~3 m depth in IP3, shows velocities of 132–139 m/s. SU2 (shown on Figure 2 – right) exhibits a wider range (198–354 m/s), reflecting material heterogeneity. In both IP2 and IP3, velocity increases with depth to ~7 m, followed by a velocity inversion between 7–8 m, with a minimum of 289 m/s in IP2 and 198 m/s in IP3. This inversion indicates a weaker, more compressible layer warranting further consideration in liquefaction assessment. Details of the test setup, data processing, and results are shown in Figure 2.

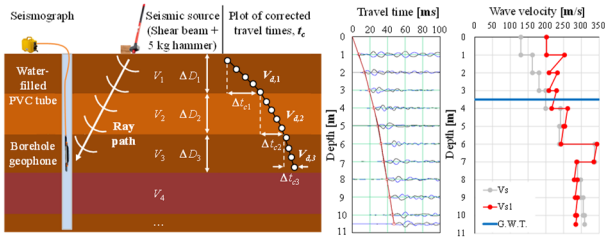

Figure 2. Down-hole seismic method for IP2: (left) testing setup and velocity calculation; (middle) corrected seismograms with S-wave first-break picks; (right) V_s and normalized V_{s1} profiles.

3 LIQUEFACTION ASSESSMENT

The assessment of soil liquefaction hazard typically follows a structured workflow (Figure 3):

1. Establish composition-based susceptibility criteria using fines content, plasticity, and related index properties.
2. Perform triggering analysis to estimate the likelihood of liquefaction under the design earthquake.
3. Evaluate post-triggering effects, including settlements, stability, and deformation.
4. Decide whether mitigation is required to achieve acceptable performance.

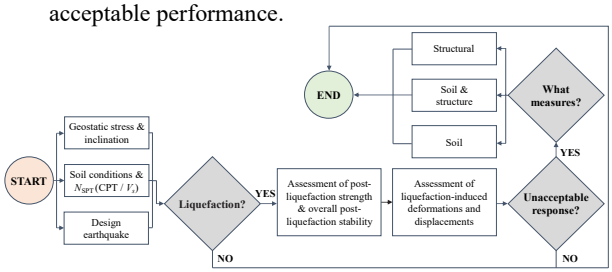

Figure 3. Flowchart of key steps in soil liquefaction assessment and mitigation (Milev, 2023).

In this paper, this procedure is applied to a shopping center site in Bulgaria, starting with susceptibility screening and progressing through triggering and settlement calculations for both Ultimate Limit State (ULS) and Damage Limitation State (DLS) conditions in accordance with Eurocode 8. Particular emphasis is placed on the use of an integrated SPT–V_s method that accounts for soil fabric effects, enabling more refined triggering assessments. The results of this innovative approach are compared with conventional SPT and V_s-based analyses, and the final design decision is presented, including the adopted mitigation strategy.

3.1 *Susceptibility*

Liquefaction susceptibility for Layer 2 and Layer 3 was evaluated using established procedures (Bray & Sancio, 2008; Iai & Matsunaga, 1990; Seed et al., 2003), based on grain-size distribution, plasticity index (IP), liquid limit (w_L), and the ratio of natural water content (w_n) to liquid limit (w_n/w_L).

Most grain-size curves for Layer 2 plot almost entirely within the “high risk” or “susceptible” zone, with only isolated cases outside or borderline. For Layer 3, all curves fall largely in the same zone. However, plasticity-based criteria classify some samples as non-liquefiable. Several samples from both layers show no plasticity, an unfavorable factor for liquefaction resistance.

These findings confirm the need for detailed seismic liquefaction assessment of both Layer 2 and the weaker interlayer (Layer 3), which is addressed in the subsequent triggering and settlement evaluation.

3.2 *Triggering and settlement evaluation*

Liquefaction triggering was assessed in parallel using two complementary approaches:

1. SPT-based method – applying the deterministic procedures of (Idriss & Boulanger, 2004) for cyclic resistance ratio (CRR) estimation, with post-liquefaction settlement calculated afterwards.
2. V_s-based method – applying the shear-wave velocity liquefaction evaluation procedure of (Andrus & Stokoe, 2000), as updated in (Andrus et al., 2004), using corrected shear wave velocities (V_{s1}) obtained from down-hole testing (see Figure 2 for V_s and V_{s1} profiles).

In both methods, the evaluation compares the cyclic stress ratio (CSR), representing the earthquake-induced seismic

demand, with the cyclic resistance ratio (*CRR*), representing the soil's resistance to liquefaction. Triggering is considered likely when *CSR* exceeds *CRR* for a given depth. The representative earthquake scenario corresponds to $M_w = 6.5$ and a design peak ground acceleration $a_g = 0.23g$, consistent with Eurocode 8 seismic hazard parameters. A safety factor of 1.35 was applied to *CRR* values in accordance with Eurocode 8, so triggering is assumed when $CSR > CRR / 1.35$.

The results show a clear trend – soils below the groundwater level, particularly between approximately -4.0 m and -6.0 m from ground level, exhibit *CSR* values greater than $CRR / 1.35$ (and Factor of Safety, $FS < 1.0$). This indicates that Layer 3 is entirely susceptible to liquefaction. In addition, Layer 2 shows partial susceptibility immediately below Layer 3.

Based on all analyses and calculations, the following general conclusions regarding liquefaction susceptibility under the design earthquake can be made:

- Layer 1 – located above the groundwater level, therefore not susceptible to liquefaction.
- Layer 3 – entirely susceptible to liquefaction.
- Layer 2 – partially susceptible to liquefaction from the base elevation of Layer 3 down to approximately -6.0 m.

These trends are illustrated in Figure 4, which shows *CSR* and *CRR* profiles from both $(N_1)_{60}$ and Vs_1 (left), the corresponding factor of safety (*FS*) profiles (middle), and post-liquefaction settlement estimates from various empirical methods (right) – (Cetin et al., 2004; Ishihara & Yoshimine, 1992; Shamoto et al., 1998; Tokimatsu & Seed, 1984; Wu, 2002). The Vs and Vs_1 profiles used in the V_s-based assessment are presented earlier in Figure 2.

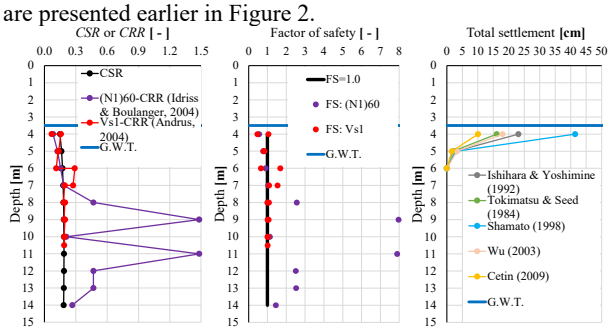

Figure 4. Liquefaction evaluation for IP2 (Ultimate Limit State – ULS): (left) *CSR* and *CRR* profiles from $(N_1)_{60}$ and V_{s1}; (middle) Factor of Safety (*FS*) profiles from SPT and V_{s1}; (right) post-liquefaction settlement from various empirical methods.

The predicted liquefaction-induced settlements are in the range of 15–25 cm when excluding extreme maximum and minimum values reported by individual authors. Such magnitudes are well beyond acceptable serviceability limits for the planned shallow foundations, confirming the need for targeted mitigation measures to ensure operational performance and safety under the design seismic loading.

In summary, both SPT- and V_s-based evaluations lead to consistent conclusions: under the Ultimate Limit State (ULS) seismic loading, there is an approximately 2 m-thick liquefiable zone between −4 m and −6 m depth, which poses a significant risk to the planned development if left untreated.

3.3 *Application of integrated SPT–Vs method*

Soil fabric is a critical factor influencing liquefaction potential. While the Standard Penetration Test (SPT) primarily reflects soil density, shear wave velocity (V_s) captures the influence of soil fabric and structure. Considering only density (via SPT) or only V_s can therefore lead to misleading results. Two soils may exhibit the same $(N_1)_{60}$ but have very different V_{s1} values, resulting in markedly different liquefaction behavior.

Recent studies (Lau et al., 2023; Lau, 2024) have introduced an integrated SPT–V_s procedure that combines the two parameters for a more accurate evaluation of liquefaction potential. Conventional methods that rely solely on SPT or solely on V_s often yield overconservative results, potentially leading to unnecessary increases in construction cost. The purpose of the integrated method is to provide a more targeted and realistic liquefaction assessment.

The procedure, illustrated in Figure 5, is as follows:

- Step 1: Determine *CRR* from SPT data – in this study, the procedure of (Boulanger & Idriss, 2014) was applied.
- Step 2: Obtain "implied V_{s1}" – using the *CRR*–relationship from the literature, e.g. (Kayen et al., 2013), the *CRR* value from Step 1 is projected onto the curve to obtain the "implied V_{s1}".
- Step 3: Calculate the "V_{s1}-ratio" which is the "in-situ V_{s1}" (derived from down-hole seismic testing in the presented study) over the "implied V_{s1}".
- Step 4: Recalculate the *CRR* (called "$CRR_{SPT\&Vs}$" below) by the equation given in Figure 5.

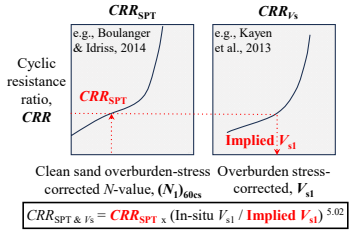

Figure 5. Proposed method combining density effect from SPT *N*-values with soil fabric from V_s measurements to obtain corrected cyclic resistance ratio ($CRR_{SPT\&Vs}$) – (Lau et al., 2023; Lau, 2024).

If the "V_{s1}-ratio" is larger than 1.0, the recalculated $CRR_{SPT\&Vs}$ will be greater than the *CRR* obtained from SPT alone. This procedure is recommended when the "V_{s1}-ratio" falls between 0.8 and 1.2, which is the range supported by current experimental data.

For this study, the integrated method was applied. The analysis yielded $CRR_{SPT\&Vs} \approx 2.5 \times CRR_{SPT}$, which exceeds the cyclic stress ratio (*CSR*) for the Ultimate Limit State (ULS) earthquake scenario. This outcome indicates that, when assessed with the integrated SPT–V_s procedure, the soil profile is not expected to undergo liquefaction even under ULS loading.

The application of the integrated SPT–V_s method has important design implications. While traditional SPT- or V_s-only approaches indicated the presence of liquefiable layers requiring mitigation, the combined analysis suggests that these layers possess higher liquefaction resistance due to favorable soil fabric. This can reduce the likelihood of overdesign, enabling optimization of ground improvement measures and potentially lowering project costs without compromising safety. However, it should be noted that the method is relatively new, and further research, experimental validation, and field evidence are needed to fully confirm its reliability across different soil types and seismic conditions.

3.4 *Performance under ULS and DLS (Eurocode 8)*

Under the Ultimate Limit State (ULS) seismic loading scenario, both SPT- and V_s-based evaluations indicate the presence of a liquefiable zone approximately 2 m thick, located between -4 m and -6 m depth beneath the planned foundation level. This zone poses a potential risk to structural stability if left untreated. For the Design Limit State (DLS), no liquefaction is predicted, meaning that non-critical areas such as parking zones and supermarket flooring can be left without ground improvement. This targeted approach allows optimization of construction

resources while ensuring that life-safety requirements remain the top priority.

Additional confidence in this assessment comes from the application of the integrated SPT–V_s method, which suggests that even under ULS conditions liquefaction is unlikely due to favorable soil fabric. Nevertheless, following the decision-making framework outlined in Figure 3, soil improvement is still considered essential to guarantee structural performance and avoid collapse in the event of a strong earthquake – particularly given the relatively high seismic hazard for this part of Europe.

To address the identified ULS liquefaction hazard beneath the foundations, the deep soil mixing (DSM) method has been selected for ground improvement. Details of its design and implementation are discussed in a subsequent section.

4 LIQUEFACTION MITIGATION BY DEEP SOIL MIXING (DSM)

A comprehensive technical and economic analysis was carried out to determine the most suitable soil improvement technique for the site, ensuring both safety and cost-effectiveness under the project's design conditions.

4.1 *Selection of improvement method*

Two primary ground improvement options were shortlisted for mitigating liquefaction risk under the ULS:

1. Removal of the liquefiable layer and replacement with a dense gravel–sand cushion, which would require extensive dewatering.
2. Application of the Deep Soil Mixing (DSM) method (Kitazume & Terashi, 2013).

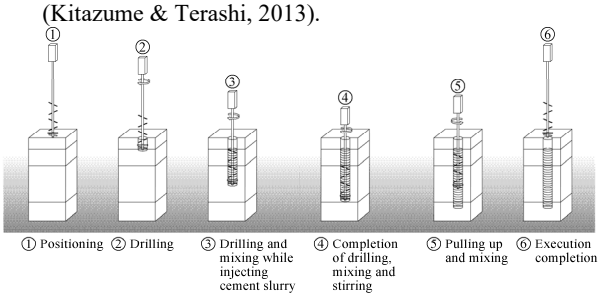

Figure 6. Execution sequence of the deep soil mixing (DSM) method (Milev, 2023).

The technical and economic assessment revealed that the dewatering and replacement option would be significantly more costly and logistically challenging due to the site's groundwater conditions. In contrast, DSM offered a more practical, reliable, and cost-efficient solution while achieving the required seismic stability improvements. Consequently, DSM was selected as the preferred method for this project, with the execution process illustrated in Figure 6.

DSM is a ground improvement method that involves mechanically blending in-situ soils with cement-based stabilizing agents to form stiff, solidified soil–cement columns. The process is typically executed using a rotating auger or mixing blades attached to a drill rig, capable of reaching depths of 20 m or more. During penetration, cement slurry is injected, and mixing occurs both on the way down and during withdrawal to ensure a homogeneous treated column. Once cured, the treated soil exhibits significantly increased shear strength, reduced compressibility, and greatly improved resistance to liquefaction. For liquefaction mitigation, DSM can be implemented in different patterns, such as block or lattice (grid) arrangements, with the block type providing the highest effectiveness by leaving no untreated zones within the target area.

In this project, DSM is applied as discrete rigid inclusions rather than a continuous block: for each 3.2 x 3.2 m footing, two sets of three secant columns (triple-system, executed simultaneously) are installed (six columns per footing) forming two overlapping tripods that start immediately below the foundation base and extend to a depth of 4.5 m. These columns pass entirely through the liquefiable layer and penetrate into the underlying non-liquefiable soil, ensuring both vertical support and lateral resistance under ULS conditions while allowing surrounding soil to remain untreated.

4.2 *Design and analysis*

The foundation system comprises mainly isolated spread footings, with strip footings applied only in localized zones. The principal columns are supported by square pads (3.20 x 3.20 m), while smaller steel columns rest on 1.00 x 1.00 m footings. All foundations are positioned at approximately -2.20 m depth, with a uniform thickness of 0.60 m.

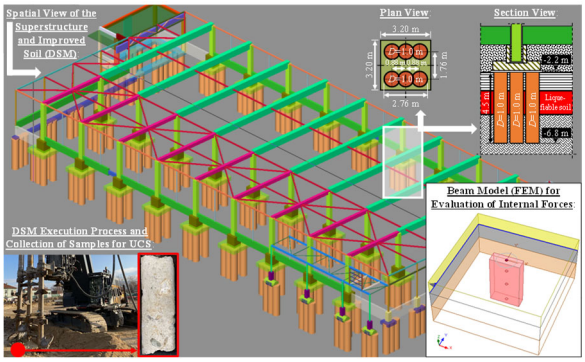

Figure 7. Overview of soil improvement design and implementation using the Deep Soil Mixing (DSM) method.

Given the liquefaction susceptibility, ground improvement was introduced beneath the most critical load-bearing elements. The adopted approach employs the Deep Soil Mixing (DSM) method (Figure 7) to form reinforced soil bodies capable of maintaining strength and stiffness during seismic loading. Triple-overlapping columns were arranged directly beneath each footing, extending through the liquefiable layer and penetrating into underlying non-liquefiable soils. Design control measures included verification of the binder mix formulation, monitoring of execution parameters, and post-installation laboratory testing of treated samples to ensure that target unconfined compressive and tensile strengths were achieved.

The basic structural FEM model includes both the superstructure and foundations. Pad and strip footings were represented as shell elements, with soil–structure interaction approximated by frame elements supported on linear springs. For the layer susceptible to liquefaction, the Winkler springs were disabled. This provided only a preliminary insight, as it could not capture key liquefaction phenomena such as effective stress reduction and excess pore pressure build-up during seismic shaking. An similar additional structural–foundation model was prepared in three variants (Figure 8):

1. Fully fixed base.
2. Improved ground using DSM.
3. Liquefied condition for critical soil layer.

This modelling aimed to quantify the inertial forces transferred from the superstructure, through the foundations, into the improved soil medium. Soil–structure interaction was incorporated using internationally recognized methods (Federal Emergency Management Agency, 2000; Gazetas & Tassoulas, 1987; Gazetas et al., 1985), which model rigid shallow foundations with vertical, horizontal, and rotational springs. Stiffness adjustments account for foundation shape,

embedment depth, and the contribution of vertical sidewalls. While the method has known limitations (such as assuming constant stiffness, neglecting coupling between load components, and ignoring uplift/rocking) it remains widely used in international practice.

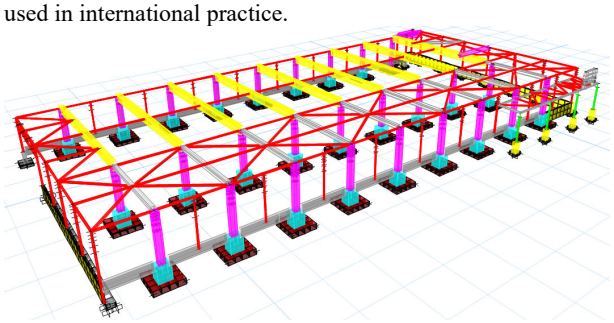

Figure 8. Simplified FEM superstructure model with spring supports for SSI representation.

For the liquefiable layer, cyclic shear stresses were estimated considering site-specific seismic hazard parameters, overburden conditions, and depth-dependent stiffness degradation. Shear wave velocity measurements (as per Figure 2) within the DSM treatment depth were used to calculate the small-strain shear modulus of the untreated soil. The stiffness of the liquefied state was derived by applying an 80% reduction to this modulus, consistent with the recommendations of (Madabhushi et al., 2009). For the DSM material, a representative shear modulus of 400 MPa was adopted in line with the values reported by (Kitazume & Terashi, 2013) and corroborated by international project experience.

Given that two DSM columns were installed beneath each footing, the improved area ratio beneath the foundation footprint was about 50%, exceeding the threshold where the soil mass can be considered a composite medium rather than discrete inclusions. The equivalent composite stiffness was calculated from the improvement ratio and the respective stiffnesses of the liquefied soil and DSM material (Figure 9). The same approach was used to determine an equivalent Poisson's ratio for the improved mass.

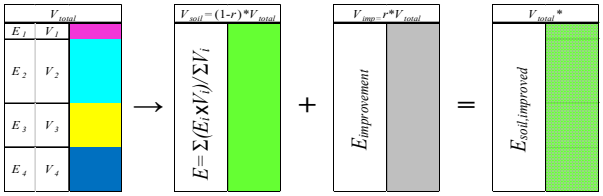

Figure 9. Schematic representation of soil improvement, showing: E_1–E_4 – deformation moduli of individual soil layers; V_1–V_4 – volumes of soil layers; V_{total} – total soil volume before improvement; V_{soil} – soil volume after improvement; V_{imp} – volume of improved zone; r – improvement ratio; $E_{improvement}$ – deformation modulus of the improvement material; $E_{soil,improved}$ – deformation modulus of the improved composite medium.

Spring constants were then computed for both liquefied and improved conditions. Results indicated that liquefaction-related stiffness degradation produced only a modest increase in the fundamental vibration periods (7–13%), suggesting that the column flexural stiffness rather than foundation rotation governed the overall dynamic response. With DSM improvement, periods and seismic response closely matched those of the fixed-base model, confirming the effectiveness of the adopted measures.

In this study, the DSM columns were also considered as discrete structural elements within the foundation soil, behaving in a manner similar to unreinforced piles. This approach allowed assessment of their performance under seismic conditions where liquefaction could occur. Experience from past earthquakes, has shown that pile damage in liquefied soils often results not only from inertial forces transmitted from the superstructure but also from significant ground deformations. Of particular concern is lateral spreading, where large, unidirectional soil displacements develop after liquefaction. This phenomenon is frequently underestimated in design, yet it can govern the structural response of pile-like elements during strong seismic events.

The interaction between soil and such elements evolves during an earthquake. Initially, cyclic strains in the soil combine with inertial forces from the superstructure to produce horizontal loading on the columns. Once liquefaction is triggered, inertial effects diminish while ground movements increase, with lateral spreading becoming the dominant loading mechanism. In this project, lateral spreading displacements were evaluated using both shear wave velocity data and SPT-based correlations (Andrus et al., 2004; Zhang et al., 2004), supported by site-specific cyclic stress ratio (*CSR*) and cyclic resistance (*CRR*) estimates (as per Figure 4). The two independent approaches produced comparable results, with average displacements of 13.16 cm and 11.07 cm respectively. For the final design assessment, the more conservative value of 13.16 cm was adopted.

The horizontal response of the DSM elements was evaluated by treating them as unreinforced pile-like members embedded in the soil, where the soil resistance is a nonlinear function of pile deflection. This relationship is typically expressed through *p–y* curves, which define soil reaction as a function of horizontal displacement at various depths. For the liquefiable layer, a hybrid liquefied sand model was adopted, following the framework of (Franke & Rollins, 2013; Rollins et al., 2005; Wang et al., 2008). This approach is suitable for soils exhibiting mixed characteristics rather than clean sands, and it accounts for the lower of two possible resistance envelopes, reflecting either liquefied sand or soft clay behavior.

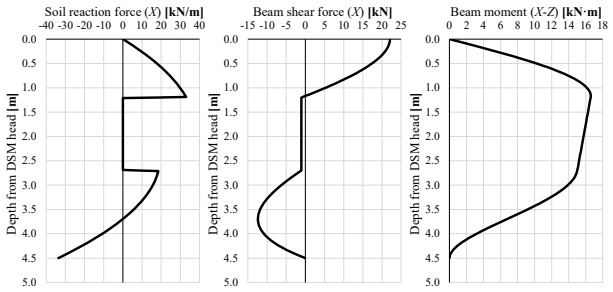

Figure 10. FEM-based beam model analysis of the DSM columns (see Figure 7 – bottom-right): (left) soil reaction force, (middle) shear force, and (right) bending moment profiles under inertial loading from the superstructure.

Two representative DSM cases were analyzed: one located where the liquefiable layer reached its maximum thickness, and another subjected to the highest shear forces transferred from the superstructure. Both inertial loading from the superstructure and kinematic loading due to lateral spreading were examined along the principal *X* and *Y* directions. The DSM bodies were represented by equivalent rectangular sections with the same stiffness characteristics as the actual triple-column geometry. Under inertial loading, soil–structure interaction springs were defined according to an enhanced Winkler-type model. For lateral spreading, the displacements calculated earlier in the study were applied directly, with stiffness adjustments for the overlying non-liquefiable layer.

The FEM-based beam model (Figure 10) provided the soil reaction, shear force, and bending moment profiles for each loading condition. The analysis indicated maximum tensile

stresses in the DSM elements of approximately 0.4 MPa and peak shear forces of about 160 kN. During construction, core samples were taken from the executed DSM columns, and their unconfined compressive strength (UCS) was determined in the laboratory. Assuming a tensile strength equal to 10% of the measured UCS, the results confirmed values slightly above the target strength specified in the design, thereby validating the adequacy of the adopted mix and execution methodology.

4.3 *Execution*

The DSM works were carried out using a LIEBHERR LRB355.1 120T rig with a 3MA 35 triple-auger tool, forming 1.0 m diameter soil–cement columns with 0.12 m overlap (center spacing of 0.88 m) beneath each foundation (Figure 6 – bottom-left). Key machine specs included: torque 35/17.5 kNm, rotation speed 62/124 rpm, max depth 30 m, and max extraction force 400 kN. Specialized equipment (binder silos, high-pressure pump, and slurry mixing unit) was mobilized, and all improvement works were completed within a couple of weeks. The rig automatically logged parameters such as rotation speed, penetration rate, binder volume, and mixing repetitions at each depth, with the recorded data subsequently reviewed by the responsible supervisory team.

5 CONCLUSIONS

This study presented an integrated workflow for assessing and mitigating liquefaction hazards beneath shallow foundations, combining detailed site investigation, performance-based evaluation under ULS and DLS seismic demands, and targeted ground improvement. Liquefaction potential was evaluated through in-situ data, supplemented by V_S-profiling, enabling a realistic characterization of soil behavior under seismic loading. The proposed methodology for treatment selection was based on load-critical locations, with DSM columns designed to penetrate critical layers and anchor into non-liquefiable strata. Advanced FEM beam modelling incorporating soil–structure interaction was applied to capture both inertial and kinematic demands, while stiffness parameters reflected measured soil and DSM properties. Execution quality was ensured through rigorous monitoring and post-installation UCS verification, confirming strengths at or slightly above design values. The work contributes to geotechnical engineering by demonstrating a practical, performance-based framework that links liquefaction assessment, seismic design principles, and construction quality control, providing a replicable approach for enhancing foundation resilience in liquefiable soils.

6 REFERENCES

Andrus, R.D., and Stokoe, K.H. II. 2000. Liquefaction resistance of soils from shear-wave velocity. *Journal of Geotechnical and Geoenvironmental Engineering*, ASCE, 126(11), 1015–1025.

Andrus, R.D., Stokoe, K.H. II, and Juang, C.H. 2004. Guide for shear-wave-based liquefaction potential evaluation. *Earthquake Spectra*, 20(2), 285–308.

ASTM D7400-19. 2019. *Standard Test Methods for Downhole Seismic Testing*. ASTM International, West Conshohocken, PA, 14 p.

Boulanger, R.W., and Idriss, I.M. 2014. *CPT and SPT based liquefaction triggering procedures*. Report No. UCD/CGM-14/01, Center for Geotechnical Modeling, Department of Civil and Environmental Engineering, University of California, 134 p.

Bray, J.D., and Sancio, R.B. 2008. Closure to "Assessment of the liquefaction susceptibility of fine-grained soils" by Jonathan D. Bray and Rodolfo B. Sancio. *Journal of Geotechnical and Geoenvironmental Engineering*, ASCE, 134(7), 1031–1034.

Cetin, K.O., Seed, R.B., Der Kiureghian, A., Tokimatsu, K., Harder, L.F. Jr, Kayen, R.E., and Moss, R.E.S. 2004. Standard penetration test-based probabilistic and deterministic assessment of seismic soil liquefaction potential. *Journal of Geotechnical and Geoenvironmental Engineering*, ASCE, 130(12), 1314–1340.

ECS – European Committee for Standardization. 2004. *Eurocode 8: Design of structures for earthquake resistance – Part 5: Foundations, retaining structures and geotechnical aspects*. EN 1998-5, Brussels: CEN.

Federal Emergency Management Agency. 2000. *Prestandard and commentary for the seismic rehabilitation of buildings – FEMA 356*. Washington, D.C.

Franke, K.W., and Rollins, K.M. 2013. Simplified hybrid p–y spring model for liquefied soils. *Journal of Geotechnical and Geoenvironmental Engineering*, ASCE, 139(4), 564–576.

Gazetas, G., and Tassoulas, J.L. 1987. Horizontal stiffness of arbitrarily shaped foundations. *Journal of Geotechnical Engineering*, ASCE, *113*(5), 440–457.

Gazetas, G., Dobry, R., and Tassoulas, J.L. 1985. Vertical response of arbitrarily shaped embedded foundations. *Journal of Geotechnical Engineering*, ASCE, *111*(6), 750–771.

Iai, S., and Matsunaga, Y. 1990. Study on shear stress ratio in liquefaction assessment. *Proceedings of the 25th Japanese National Conference on Soil Mechanics and Foundation Engineering*, 773–776 (in Japanese).

Idriss, I.M., and Boulanger, R.W. 2004. Semi-empirical procedures for evaluating liquefaction potential during earthquakes. *Proceedings of the 11th International Conference on Soil Dynamics and Earthquake Engineering and 3rd Int. Conference on Earthquake Geotech. Engineering*, Vol. 1, 32–56. Singapore: Stallion Press.

Ishihara, K., and Yoshimine, M. 1992. Evaluation of settlements in sand deposits following liquefaction during earthquakes. *Soils and Foundations*, 32(1), 173–188.

Kayen, R.E., Moss, R.E.S., Thompson, E.M., Seed, R.B., Cetin, K.O., Der Kiureghian, A., Tanaka, Y., and Tokimatsu, K. 2013. Shear-wave velocity–based probabilistic and deterministic assessment of seismic soil liquefaction potential. *Journal of Geotechnical and Geoenvironmental Engineering*, ASCE, 139(3), 407–419.

Kitazume, M., and Terashi, M. 2013. *The deep mixing method* (Vol. 21). London: CRC Press.

Lau, K. K., Kiyota, T., Shiga, M., and Hsieh, P.C. 2023. Investigation of soil density and fabric effect on SPT and Vs measurements using a calibration chamber. *Seisan Kenkyu*, 75(4), 269–273.

Lau, K. K. 2024. *Evaluation of liquefaction triggering potential using SPT and Vs data*. Doctoral thesis, Department of Civil Engineering, The University of Tokyo, Tokyo, Japan, 176 p.

Madabhushi, G., Haigh, S., and Knappett, J. 2009. *Design of pile foundations in liquefiable soils*. World Scientific.

Milev, N. 2023. *Soil liquefaction countermeasures*. Sofia: Kolbis International Transfer Corp., 208 p. ISBN 978-619-7691-61-0.

Nakov, R., and Dobrev, N. 2014. Geological risk assessment methodology. Report for Ministry of Regional Development and Public Works of Bulgaria.

Rollins, K.M., Gerber, T.M., Lane, J.D., and Ashford, S.A. 2005. Lateral resistance of a full-scale pile group in liquefied sand. *Journal of Geotechnical and Geoenvironmental Engineering*, ASCE, 131(1), 115–125.

Seed, R.B., Cetin, K.O., Moss, R.E.S., Kammerer, A.M., Wu, J., Pestana, J.M., Riemer, M.F., Sancio, R.B., Bray, J.D., Kayen, R.E., and Faris, A. 2003. Recent advances in soil liquefaction engineering: a unified and consistent framework. *Proceedings of the 26th Annual ASCE Geotechnical Spring Seminar*, California.

Shamoto, Y., Zhang, J.M., and Tokimatsu, K. 1998. New charts for predicting large residual post-liquefaction ground deformation. *Soil Dynamics and Earthquake Engineering*, 17(7–8), 427–438.

Tokimatsu, K., and Seed, H.B. 1984. Evaluation of settlements in sands due to earthquake shaking. *Journal of Geotechnical Engineering*, ASCE, 110(12), 1466–1487.

Wang, S.T., Vasquez, L., and Reese, L.C. 2008. Study of the behavior of pile groups in liquefied soils. *Proceedings of the 14th World Conference on Earthquake Engineering*, Beijing, China.

Wu, J. 2002. *Liquefaction triggering and post-liquefaction deformation of Monterey 0/30 sand under unidirectional cyclic simple shear loading*. PhD thesis, University of California, Berkeley.

Zhang, G., Robertson, P.K., and Brachman, R.W.I. 2004. Estimating liquefaction-induced lateral displacements using the standard penetration test or cone penetration test. *Journal of Geotechnical and Geoenvironmental Engineering*, ASCE, 130(8), 861–871.